Physics

Physics fields

Okayama University   *Year* 2002

Structure and physical properties of Cs3+alpha C60 (alpha=0.0-1.0) under ambient and high pressures

S. Fujiki[*]   Y. Kubozono[†]   M. Kobayashi[‡]

T. Kambe[**]   Y. Rikiishi[††]   S. Kashino[‡‡]

K. Ishii[§]   H. Suematsu[¶]   A. Fujiwara[‖]

[*]Department of Chemistry, Okayama University
[†]Department of Vacuum UV Photoscience, Institute for Molecular Science
[‡]Department of Materials Science, Himeji Institute of Technology
[**]Department of Physics, Okayama University
[††]Department of Chemistry, Okayama University
[‡‡]Department of Chemistry, Okayama University
[§]Department of Physics, The University of Tokyo
[¶]Department of Physics, The University of Tokyo
[‖]Japan Advanced Institute of Science and Technology

Structure and physical properties of $Cs_{3+\alpha}C_{60}$ ($\alpha=0.0-1.0$) under ambient and high pressures

S. Fujiki,[1] Y. Kubozono,[2,*] M. Kobayashi,[3] T. Kambe,[4] Y. Rikiishi,[1] S. Kashino,[1] K. Ishii,[5] H. Suematsu,[5] and A. Fujiwara[6]

[1]*Department of Chemistry, Okayama University, Okayama 700-8530, Japan*
[2]*Department of Vacuum UV Photoscience, Institute for Molecular Science, Okazaki 444-8585, Japan*
[3]*Department of Materials Science, Himeji Institute of Technology, Kamigori 678-1297, Japan*
[4]*Department of Physics, Okayama University, Okayama 700-8530, Japan*
[5]*Department of Physics, The University of Tokyo, Tokyo 113-0033, Japan*
[6]*Japan Advanced Institute of Science and Technology, Ishikawa 923-1292, Japan*

The intermediate phases $Cs_{3+\alpha}C_{60}$ ($\alpha=0.0-1.0$), have been prepared, and their structure and physical properties are studied by x-ray powder diffraction, Raman, ESR, electric conductivity, and ac susceptibility measurements under ambient and high pressures. The x-ray powder diffraction pattern of $Cs_{3+\alpha}C_{60}$ ($\alpha=0.0-1.0$) can be indexed as a mixture of the body-centered-orthorhombic (bco) and cubic ($A15$) phases. The $A15$ phase diminishes above 30 kbar. The broad ESR peak due to the conduction electron (c-ESR) is observed only for the phases around $\alpha=0.0$ in $Cs_{3+\alpha}C_{60}$. The resistivity of the $Cs_{3+\alpha}C_{60}$ ($\alpha\neq0$) sample follows the granular metal theory and/or Sheng model even in the sample exhibiting a broad ESR peak. No superconducting transition is observed up to 10.6 kbar in $Cs_{3+\alpha}C_{60}$ ($\alpha\neq0$). These results present that bco phase of $Cs_{3+\alpha}C_{60}$ ($\alpha=0$) is a final candidate for a pressure-induced superconductor.

PACS number(s): 74.70.Wz, 74.62.Fj

I. INTRODUCTION

It is well known that the superconducting transition temperature T_c in alkaline-metal-doped C_{60}, A_xC_{60} (A is an alkaline-metal atom), increases with an increase in the unit-cell volume V.[1,2] This can be related to an increase in the density of states on the Fermi level, $N(\varepsilon_F)$.[3] Therefore, it has been expected that Cs_3C_{60} should show the highest T_c among alkaline-metal-doped fullerides. Contrary to this expectation, the phase of Cs_3C_{60} was not a superconductor under ambient pressure. However, the Cs_3C_{60} phase showed a superconducting transition by applying pressure; T_c is 40 K at 12.1 kbar.[4] The Cs_3C_{60} sample could not be prepared by a normal annealing technique because the Cs_3C_{60} phase separated into Cs_1C_{60} and Cs_4C_{60} at a higher temperature than 120 °C. In 1995, Palstra *et al.* succeeded in preparing the Cs_3C_{60} sample by a liquid NH_3 synthesis technique.[4] The sample was reported to contain a body-centered-tetragonal (bct: $I4/mmm$) phase as a major phase and a simple cubic ($A15:Pm\bar{3}n$) phase as a minor phase.[4] Subsequently, Yoshida *et al.* found that Cs_3C_{60} took two phases of body-centered-orthorhombic (bco: *Immm*) and simple cubic ($A15:Pm\bar{3}n$).[5] Further, it was reported that an insulating Cs_4C_{60} takes a bco structure in the same manner as Cs_3C_{60}.[6] The difference in the structures between Cs_3C_{60} and Cs_4C_{60} is found only in an occupancy of Cs atoms: 0.75 for Cs_3C_{60} and 1.0 for Cs_4C_{60}. Therefore, we can expect an existence of intermediate phases which can be represented as $Cs_{3+\alpha}C_{60}$ ($\alpha=0.0-1.0$).

The pressure dependence of T_c in Cs_3C_{60} is contrary to that of T_c in the other superconducting fullerides. That is, T_c increases with an increase in pressure, and it reaches 40 K at 12.1 kbar.[4] Palstra *et al.* proposed three models for the pressure-induced superconductivity of Cs_3C_{60}.[4] The first model is based on the assumption that the shielding currents are suppressed by a disorder such as a fine grain and the two-phase nature of bco and $A15$. The second model as-

sumes that pressing the grains improves the connectivity of the material, and reduces the fluctuation of superconducting order parameter Ψ. The third model is based on the assumption that C_3C_{60} is a Mott-Hubbard insulator. Further, we can propose a fourth model in which pressure may induce a structural transition from the bco phase to the cubic phase. Such a structural transition may realize the superconducting phase because the superconducting transition is observed usually for the cubic phase of A_3C_{60}.

The first purpose of the present study is to search the pressure-induced superconducting phase of Cs_3C_{60}. We have searched this superconducting phase among the bco phases of $Cs_{3+\alpha}C_{60}$ ($\alpha=0.0-1.0$) and the $A15$ phase of Cs_3C_{60}. The structure and physical properties of these phases have been studied in wide temperature and pressure regions by x-ray powder diffraction, Raman, ESR, resistivity and ac susceptibility measurements. The second purpose is to pursue the mechanism of pressure-induced superconductivity based on the results obtained by the above measurements. The clarification of the mechanism should give us an indication as to the preparation of fullerene materials exhibiting higher T_c.[10]

II. EXPERIMENT

The $Cs_{3+\alpha}C_{60}$ ($\alpha=0.0-1.0$) sample was prepared by a reaction of C_{60} with Cs metal in liquid NH_3 for 1 h, NH_3 was dried with Na metal before using it. After the reaction of C_{60} and Cs metal, NH_3 was removed by a dynamical pumping under 10^{-5} Torr at 373 K. The bco-enriched sample was prepared by removing NH_3 slowly (~12 h), while the $A15$-enriched sample was prepared by removing it rapidly (~1 h). The $Cs_{3+\alpha}C_{60}$ ($\alpha=0.0-1.0$) sample was introduced into a glass capillary ($\phi=0.7$ mm) without an exposure to air in an Ar glove box in order to measure x-ray powder diffraction and Raman spectra at 1 bar. The x-ray powder diffraction patterns were measured at 298 K with Cu K_α radiation (wavelength 1.5418 Å) at 40 kV and 200 mA with a Rigaku Rint1500 x-ray diffractometer and with synchro-

tron radiation (wavelength 0.6905 Å) at BL-1B of the Photon Factory of the High Energy Acceleration Research Organization (KEK-PF), Tsukuba, Japan. The Rietveld refinements were performed by using the RIETAN-94 program for all x-ray powder diffraction patterns under ambient and high pressures.[7,8]

In order to apply hydrostatic pressure to the sample, the $Cs_{3+\alpha}C_{60}$ ($\alpha = 0.0 - 1.0$) sample was introduced into a diamond-anvil cell with mineral oil in the Ar glove box. The x-ray powder diffraction patterns were measured in a pressure region up to 50 kbar with synchrotron radiation (wavelength $= 0.6900$ Å) at BL-1B of KEK-PF. The sample pressure was determined by detecting fluorescence of ruby.[9]

The Raman scattering was measured at an excitation of 632.8 nm by a He-Ne laser with a Confocal Raman Imaging LabRam system (Jovan-Ybon). The Raman peak was analyzed by a least-squares fitting with the Breit-Wigner-Fano (BWF) formula. ESR spectra were recorded at 298 K under ambient pressure with an *X*-band ESR spectrometer (Brucker ESP300). The sample was introduced into an ESR tube without an exposure to air in the Ar glove box.

The resistivity, ρ was measured with a pellet by using a four-probe technique in a temperature region from 42 to 300 K; the measurement was performed by using a Physical Property Measurement System (Quantum Design). The gold wires were attached to the pellet with silver paste. To minimize the Joule heating effect, the excitation current was suppressed to 0.005 μA at the temperature below 75 K, to 0.5 μA at 75–100 K and to 50 μA above 100 K.

The ac susceptibility was measured by the hartshorn bridge technique. The sample was introduced into a coil without an exposure to air in the Ar glove box. The frequency of the AC magnetic field was 199 Hz. The real and imaginary parts χ' and χ'', of the complex susceptibility of the sample were measured with a two-phase lock-in detector. χ' was measured from 1.3 to 300 K under high pressure; the applied pressures were 6.9 kbar for the $Cs_{3.2(3)}C_{60}$ sample, 10.6 kbar for the $Cs_{3.3(1)}C_{60}$ sample, and 8.1 kbar for the $Cs_{3.5(1)}C_{60}$ sample. A piece of Nb was introduced into the opposite site of the sample in the coil to calibrate the temperature from the T_c of Nb, and a piece of Sn was also introduced together with Nb to estimate the pressure from the T_c of Sn. The sample was covered with fluorinert to realize hydrostatic pressure.

III. RESULTS AND DISCUSSION

The x-ray powder diffraction pattern of the $Cs_{3.5(1)}C_{60}$ sample at 298 K under ambient pressure is shown in Fig. 1, as a typical example of $Cs_{3+\alpha}C_{60}$ ($\alpha = 0.0 - 1.0$). In the present paper, the sample name is represented by the chemical composition determined for the bco phase by Rietveld refinement; "$\alpha \neq 0$" means α in the region, $0 < \alpha \leqslant 1.0$. The x-ray-diffraction pattern was indexed based on the bco and the *A*15 phases as done for $Cs_{3.00(2)}C_{60}$.[5] The fraction of the *A*15 phase in the $Cs_{3.5(1)}C_{60}$ sample was determined to be 31%; this sample is the *A*15 enriched sample. The bco $Cs_{3.5(1)}C_{60}$ has the same structure as the bco $Cs_{3.00(2)}C_{60}$ reported previously,[5] except for the occupancies of Cs atoms: $a = 11.837(7)$ Å, $b = 12.174(7)$ Å, $c = 11.456(6)$ Å, and

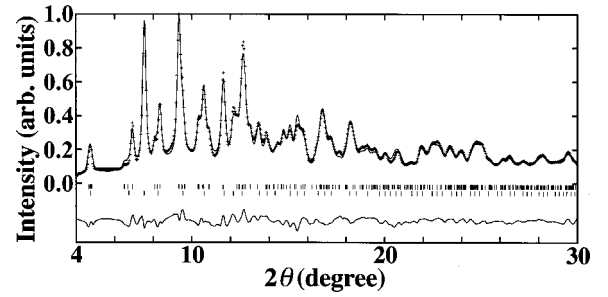FIG. 1. X-ray-diffraction pattern of the $Cs_{3.5(1)}C_{60}$ sample at 298 K and 1 bar. The crosses and solid line refer to the experimental and the best-fitted patterns, respectively. Ticks mark the positions of allowed Bragg reflections (top: the bco phase; bottom: the *A*15 phase). The difference between the experimental pattern and the best-fitted pattern is shown by the thin lines in the bottom of the figure.

$V = 1651(2)$ Å^3. The final values of weighted pattern R factor R_{wp}, and the pattern R factor R_p were 0.072 and 0.057, respectively. The structural parameters are listed in Table I.

The Rietveld refinement for the *A*15 phase (Cs_3C_{60}) in the $Cs_{3.5(1)}C_{60}$ sample was performed based on the structure of Ba_3C_{60} (Ref. 10); $a = 11.757(6)$ Å and $V = 1625(1)$ Å^3. The Cs atom can occupy either the 6*c* or 6*d* site in the *A*15 phase. The Ba atom occupies the 6*c* site in the case of Ba_3C_{60}. If the Cs atom occupies the 6*c* site as in Ba_3C_{60}, it faces the five-membered rings of C_{60} molecules [Fig. 2(a)]. On the other hand, if the Cs atom occupies the 6*d* site, it faces the six-membered rings [Fig. 2(b)]. The values of R_{wp} and R_p in the Rietveld refinement based on the 6*c* site model were 0.072 and 0.057, respectively, while those were 0.066 and 0.053 based on the 6*d* site model. The difference in R factors is too small to determine the site of the Cs atom, unequivocally though a recent theoretical study supports the 6*d* site model.[11] We carried out the Rietveld refinement based on only a 6*c* site model for all samples other than $Cs_{3.5(1)}C_{60}$, as in the case of Ba_3C_{60}. The structural param-

TABLE I. Structural parameters from Rietveld analysis for the BCO phase of $Cs_{3.5(1)}C_{60}$ at 1 bar and 298 K. The space group is *Immm*. The lattice parameters are $a = 11.837(7)$, $b = 12.174(7)$, and $c = 11.456(6)$ Å. The final weighted pattern R factor $R_{wp} = 0.072$, and the final pattern R factor $R_p = 0.057$.

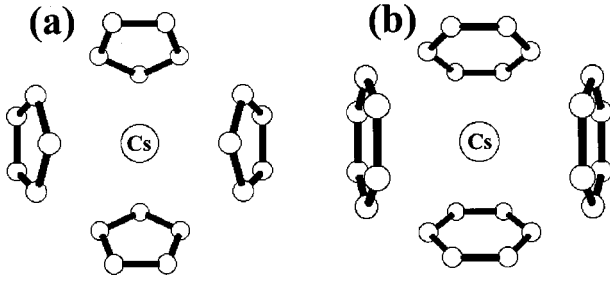|	Site	x	y	z	Occupancy	B (Å^2)
$C1$	8*l*	0	0.2862	0.0628	1.0	1.55
$C2$	8*m*	0.0608	0	0.3052	1.0	1.55
$C3$	8*n*	0.2954	0.0589	0	1.0	1.55
$C4$	16*o*	0.0984	0.2498	0.1256	1.0	1.55
$C5$	16*o*	0.1216	0.0954	0.2663	1.0	1.55
$C6$	16*o*	0.2578	0.1179	0.1017	1.0	1.55
$C7$	16*o*	0.1969	0.2133	0.0628	1.0	1.55
$C8$	16*o*	0.0608	0.1908	0.2274	1.0	1.55
$C9$	16*o*	0.2202	0.0589	0.2034	1.0	1.55
$Cs1$	4*f*	0.209(1)	0.5	0	0.86(3)	0.4(8)
$Cs2$	4*h*	0	0.255(1)	0.5	0.87(2)	0.5(8)

FIG. 2. View of the coordination around the Cs atom at (a) $6c$ and (b) $6d$ sites.

eters for the $A15$ phase are listed in Table II.

The $A_g(2)$ Raman spectrum of the $Cs_{3.5(1)}C_{60}$ sample is shown in Fig. 3. The ω_0 values were determined to be 1445 and 1451 cm^{-1} by a two-component fitting with the Breit-Wigner-Fano (BWF) formula. It is known that the ω_0 for the $A_g(2)$ mode, 1468 cm^{-1}, in pristine C_{60} shifts to lower energy by ~6 cm^{-1} for one-electron transfer from a metal atom to a C_{60} molecule.[12–14] On the other hand, the ω_0 of $A_g(2)$ mode are observed at 1450 cm^{-1} for Cs_3C_{60} (Ref. 5) and 1438 cm^{-1} for Cs_4C_{60}.[6] These results show that the $Cs_{3.5(1)}C_{60}$ sample contains both phases of $Cs_{3.4}C_{60}$ and $Cs_{3.0}C_{60}$, as expected from the x-ray powder diffraction. The fractions of $Cs_{3.4}C_{60}$ and $Cs_{3.0}C_{60}$ were determined to be 61% and 39% from the $A_g(2)$ Raman spectrum, respectively, which are consistent with the Rietveld refinement. The compositions of all samples used were confirmed by both the x-ray powder diffraction and the $A_g(2)$ Raman spectrum.

The x-ray diffraction pattern of $Cs_{3.00(6)}C_{60}$ at 1 bar was indexed with the bco and $A15$ phases; the fraction of the $A15$ phase was 2%.[5] a, b, c, and V for the bco phase at 1 bar were 11.843(7), 12.220(7), 11.464(6) Å, and 1659(2) Å^3, respectively. The x-ray diffraction pattern at 20 kbar was indexed with two phases of bco and $A15$.[15] a, b, c, and V for the bco phase at 20 kbar were 11.51(2), 11.97(2), 11.43(2) Å, and 1575(4) Å^3, respectively. The x-ray diffraction pattern at 49 kbar showed no peak due to the $A15$ phase. This pattern could be indexed only with the bco structure.[15] a, b, c, and V at 49 kbar were 11.06(8), 11.69(8), 11.45(8) Å, and 1482(18) Å^3, respectively. The pressure dependence of a, b, and c in the bco $Cs_{3.00(6)}C_{60}$ is shown in Fig. 4(a), and that of V is shown in Fig. 4(b). All lattice constants decrease monotonously with an increase in pressure. The compressibility κ for a is 2.0×10^{-3} kbar^{-1}, which is larger than those for b (6.3×10^{-4} kbar^{-1}) and c (1.8×10^{-4} kbar^{-1}). κ for V is estimated to be 3.1×10^{-3} kbar^{-1}, which is similar to those
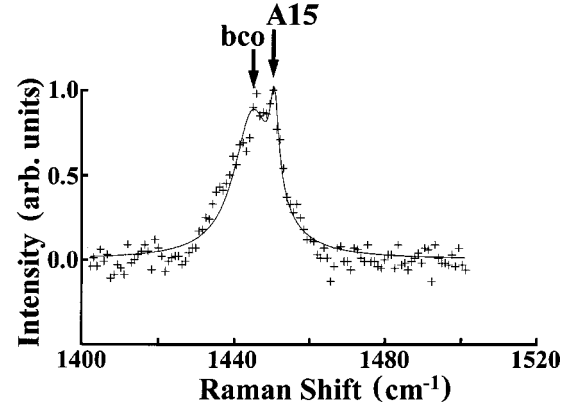

FIG. 3. $A_g(2)$ Raman peak of the $Cs_{3.5(1)}C_{60}$ at 298 K and 1 bar. The crosses and solid line refer to the experimental and the best-fitted patterns, respectively. The Raman peak was analyzed by two BWF formula.

for K_3C_{60} and Rb_3C_{60} (4.08×10^{-3} kbar^{-1}).[1]

The x-ray-diffraction patterns for the $Cs_{3.5(1)}C_{60}$ sample at 20 and 50 kbar are shown in Figs. 5(a) and 5(b), respectively; the fraction of the $A15$ phase was 31% at 1 bar (Fig. 1). a, b, c, and V for the bco phase of $Cs_{3.5(1)}C_{60}$ were 11.24(3), 11.91(3), 11.43(2) Å, and 1530(6) Å^3, respectively, at 20 kbar, and 10.98(3), 11.53(3), 11.45(4) Å, and 1450(8) Å^3 at 50 kbar. R_{wp} and R_p were 0.056 and 0.043, respectively, at 20 kbar, and 0.044 and 0.028 at 50 kbar. On the other hand, a and V for the $A15$ phase were 11.42(3) Å and 1489(6) Å^3, respectively, at 20 kbar, and 11.4(2) Å and 1495(55) Å^3 at 50 kbar. The fractions of the $A15$ phase were 15% at 20 kbar and 1% at 50 kbar. This result shows that the $A15$ phase disappears in the high-pressure region. The fraction of the $A15$ phase decreased with an increase in pressure, while no structural transition for the bco phases of $Cs_{3.00(6)}C_{60}$ and $Cs_{3.5(1)}C_{60}$ was observed under high pressure.

The κ values of a, b, c, and V for the bco phase of the $Cs_{3.5(1)}C_{60}$ sample, 1.4×10^{-3}, 1.0×10^{-3}, 5.3×10^{-6}, and 2.5×10^{-3} kbar^{-1}, respectively, are similar to those for $Cs_{3.00(6)}C_{60}$, i.e., the bco phase of $Cs_{3+a}C_{60}$ is hardly compressed along the c axis. Further, the increase in the occupancies of the Cs atoms reduces the κ of V. The pressure dependence of a and the fraction of the $A15$ phase in the
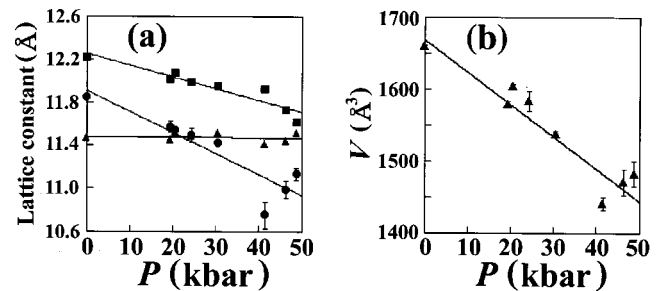
TABLE II. Structural parameters from Rietveld analysis ($6c$ site model) for the $A15$ phase of Cs_3C_{60} at 1 bar and 298 K. The space group is $Pm3n$. The lattice parameter is $a=11.757(6)$ Å.

	Site	x	y	z	Occupancy	B (Å^2)
$C1$	$24k$	0	0.3024	0.0623	1.0	3(2)
$C2$	$48l$	0.1245	0.1008	0.2639	1.0	3(2)
$C3$	$48l$	0.0623	0.2015	0.2253	1.0	3(2)
Cs	$6c$	0.25	0	0.5	1.0	0.3(4)

FIG. 4. Pressure dependence of (a) a, b and c, and (b) V of the bco phase in the $Cs_{3.00(6)}C_{60}$ sample. In (a), the symbols, ●, ■, and ▲, refer to a, b, and c, respectively. The lines refer to the best-fitted ones.
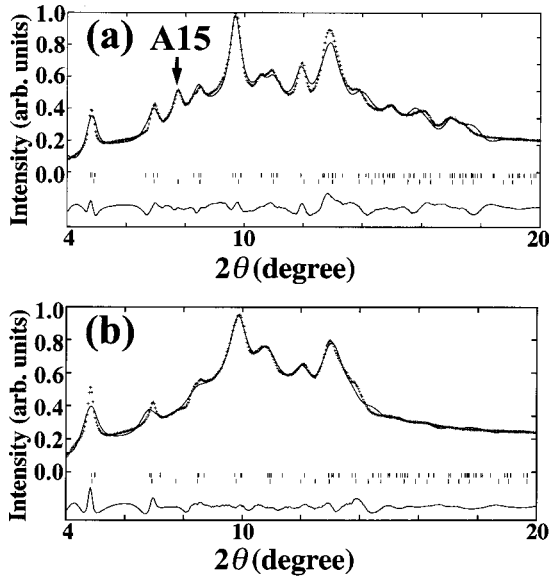
FIG. 5. X-ray powder diffraction of the $Cs_{3.5(1)}C_{60}$ sample at 298 K under pressures of (a) 20 and (b) 50 kbar. The crosses and solid lines refer to the experimental and best-fitted patterns, respectively. Ticks mark the positions of allowed Bragg reflections (top: the bco phase; bottom: the $A15$ phase). The difference between the experimental and the best-fitted patterns is shown by the thin lines in the bottom of each figure.

FIG. 6. Pressure dependence of (a) a and (b) *fractions* of the $A15$ phase in the $Cs_{3.5(1)}C_{60}$ sample.
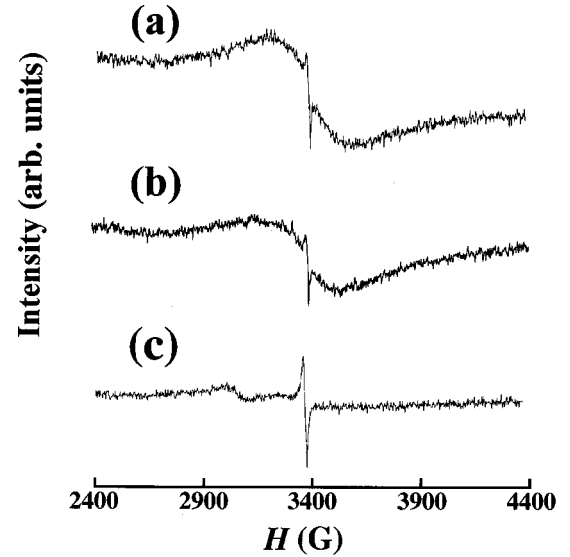
FIG. 7. ESR spectra of (a) the $Cs_{3.00(6)}C_{60}$, (b) $Cs_{3.3(1)}C_{60}$, and (c) $Cs_{3.4(2)}C_{60}$ samples at 298 K and 1 bar.

$Cs_{3.5(1)}C_{60}$ sample are shown in Figs. 6(a) and 6(b), respectively. a decreases rapidly with an increase in pressure up to 20 kbar; and becomes constant above 20 kbar, while the fraction of the $A15$ phase decreases gradually with an increase in pressure up to 30 kbar, and the phase vanishes above 30 kbar. The pressure-induced structural transition, i.e., the disappearance of the $A15$ phase, is clearly found in the plots [Fig. 6(b)]. The κ values determined from the pressure dependence below 30 kbar [Fig. 6(a)] are 1.5×10^{-3} and 4.5×10^{-3} kbar^{-1} for a and V, respectively, being the same order as those for the bco phase.

No $A15$ phase was observed in the x-ray diffraction patterns of the $Cs_{3.2(2)}C_{60}$ sample under a pressure of 40 kbar at 101 and 11 K as well as 298 K; this sample contains 5% of the $A15$ phase at 1 bar.[16] The Rietveld refinements were achieved only with the bco phase. a, b, c, and V for the bco phase were 11.8(1), 11.3(1), 11.4(1) Å, and 1521(25) Å^3, respectively, at 101 K, and 11.8(1), 11.32(9), 11.40(9) Å, and
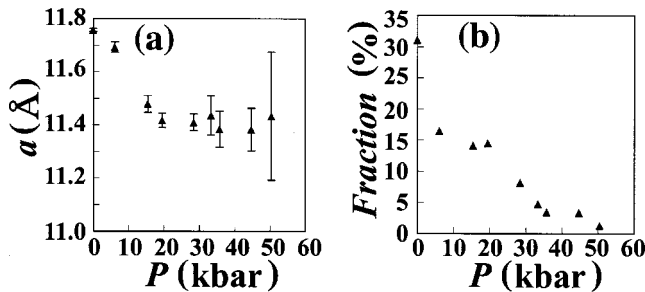
1520(23) Å^3 at 11 K.[16] These x-ray diffraction patterns show no structural transition between 101 and 11 K under a pressure of 40 kbar. Because the $A15$ phase disappears under high pressure, it can be pointed out that the pressure-induced superconducting phase of $Cs_{3+a}C_{60}$ ($a=0.0-1.0$) is not the $A15$ phase.

The electron-phonon coupling constant λ, was estimated from the Raman scattering for the $Cs_{3.2(2)}C_{60}$ sample with 5% of the $A15$ phase.[16] λ's for the $H_g(1)$ and $H_g(2)$ modes at 1 bar were estimated to be 0.08 and 0.15, respectively.[16] The contribution of the $A_g(1)$ and $A_g(2)$ modes to λ was extremely small at 1 bar in comparison with the $H_g(1)$ and $H_g(2)$ modes.[16,17] The total λ was estimated to be 0.23. This λ cannot result in a meaningful T_c based on the McMillan formula. The total λ of this sample decreases rapidly up to 30 kbar, and increases above 30 kbar.[16] This result may be associated with the phase transition from the two phases (bco and $A15$) to the single phase (bco) under high pressure. λ at 60 kbar increased to 0.25–0.3. However, the λ was still smaller than that, ~0.65, expected for $T_c=40$ K from the McMillan formula with the Coulomb repulsion, $u^*=0.1$.[16]

The ESR spectra of the $Cs_{3.00(6)}C_{60}$, $Cs_{3.3(1)}C_{60}$, and $Cs_{3.4(2)}C_{60}$ samples at 298 K are shown in Figs. 7(a), 7(b), and 7(c), respectively; the fractions of the $A15$ phase are 2% for the $Cs_{3.00(6)}C_{60}$ sample, 12% for $Cs_{3.3(1)}C_{60}$, and 20% for $Cs_{3.4(2)}C_{60}$. The ESR spectra of the $Cs_{3.00(6)}C_{60}$ sample are composed of three components one with a very narrow peak (linewidth, $\Delta H_{pp}\sim2$ G), one with a narrow peak ($\Delta H_{pp}\sim15$ G), and one with a broad peak ($\Delta H_{pp}\sim380$ G). The broad peak is close to that of Rb_3C_{60}, 490 G,[18] which is assigned to the ESR due to conduction electron (c-ESR). ΔH_{pp} of the broad peak showed a linear increase with an increase in temperature.[5] Further, the spin susceptibility χ_{spin} of $Cs_{3.00(6)}C_{60}$ showed a Pauli-paramagnetic behavior from 1.9 to 300 K, as expected for the normal metal.[5] Therefore, we assigned the broad ESR peak to c-ESR in Ref. 5.

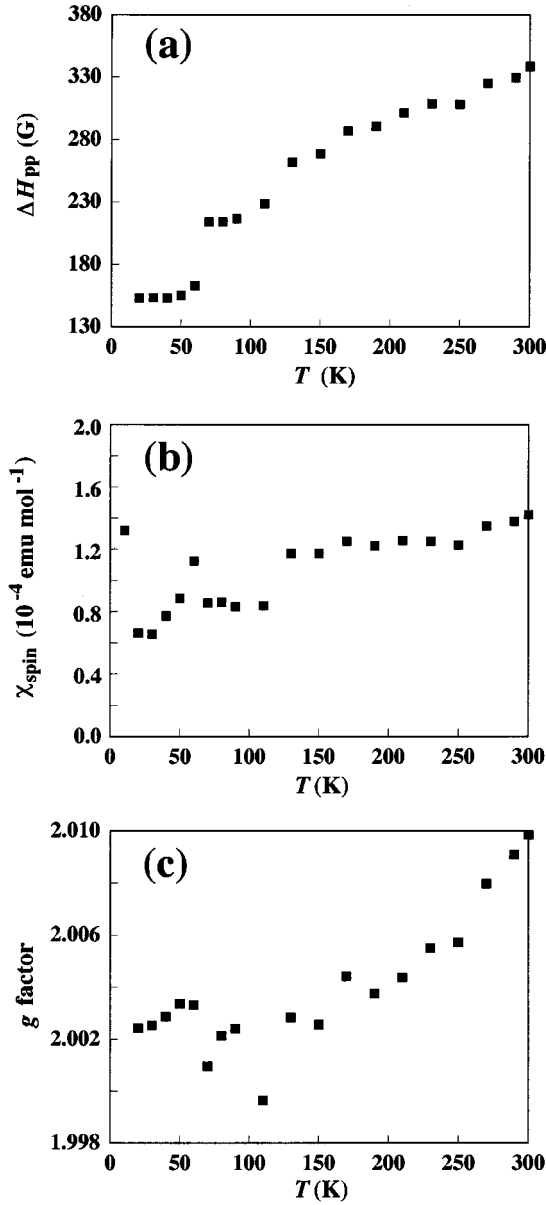The ESR spectrum of $Cs_{3.3(1)}C_{60}$ is similar to that of

FIG. 8. Plots of (a) ΔH_{pp} vs T, (b) χ_{spin} vs T, and (c) g factor vs T for the broad ESR peak in $Cs_{3.3(1)}C_{60}$.

FIG. 9. Plots of (a) ρ vs T, (b) $\ln \rho$ vs $1/T$, (c) $\ln \rho$ vs $1/T^{1/2}$, and (d) ρ vs T in $Cs_{3.5(1)}C_{60}$. In (c) and (d), the fitting curves are drawn based on the equations of granular metal theory and the Sheng model, respectively.

$Cs_{3.00(6)}C_{60}$, as shown in Fig. 7. ΔH_{pp} are very narrow, narrow, and broad peaks in $Cs_{3.3(1)}C_{60}$ are ~1, ~13, and ~340 G, respectively. The temperature dependences of ΔH_{pp} and χ_{spin} of the broad peak in $Cs_{3.3(1)}C_{60}$ are shown in Figs. 8(a) and 8(b), respectively, which are similar to that of $Cs_{3.00(6)}C_{60}$.[5] χ_{spin} shows a Pauli-paramagnetic behavior from 10 to 300 K, while the ΔH_{pp} shows a linear relationship, as in the case of $Cs_{3.00(6)}C_{60}$. We estimated $\Delta H_{pp}/(\Delta g)^2$ ($\Delta g = g - 2.0023$) because the plots should be linear for a normal metal, in which the temperature dependence of $\Delta H_{pp}/(\Delta g)^2$ is proportional to the resistivity ρ, according to the Elliott-Yafet relation.[19,20] The plots of $\Delta H_{pp}/(\Delta g)^2$, estimated with the observed g values [Fig. 8(c)] did not show a linear relationship. This may reflect the fact that it was difficult to determine the g value at high accuracy because the peak is very broad. Consequently, we
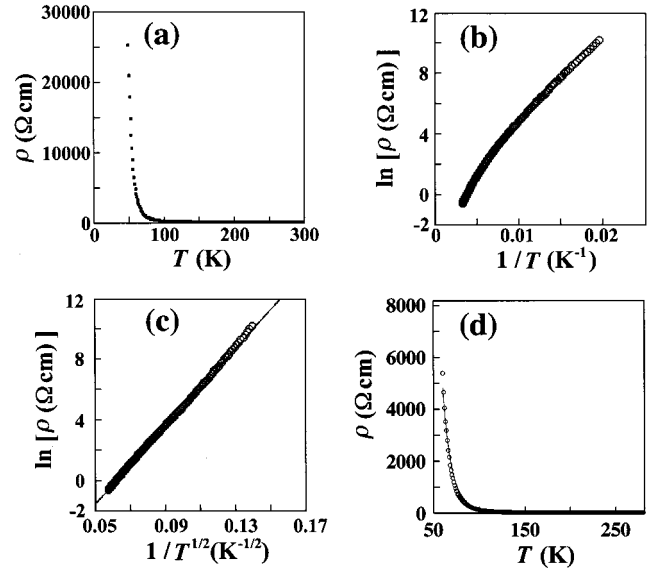
cannot definitely conclude that $Cs_{3.00(6)}C_{60}$ and $Cs_{3.3(1)}C_{60}$ are metallic, though the possibility is suggested from the temperature dependence of ΔH_{pp} and χ_{spin}.

On the other hand, the ESR spectrum of the $Cs_{3.4(2)}C_{60}$ sample showed no broad peak ascribable to c-ESR, as seen from Fig. 7(c). The ESR spectrum is composed of a narrow peak ($\Delta H_{pp} \sim 14$ G). The broad peak was not substantially found in $Cs_{3+\alpha}C_{60}$ ($\alpha \neq 0.0$) samples, though it was observed in some $Cs_{3+\alpha}C_{60}$ samples ($\alpha \sim 0.0$), as in $Cs_{3.3(1)}C_{60}$. This implies that the bco phase of $Cs_{3+\alpha}C_{60}$ ($\alpha \neq 0.0$) is not a normal metal. Further, the results of ESR suggest that the $A15$ phase is also not a normal metal because the $Cs_{3.4(2)}C_{60}$ sample contains 20% of the $A15$ phase.

The temperature dependence of the resistivity ρ for the $Cs_{3.5(1)}C_{60}$ sample is shown in Figs. 9(a); the ESR of this sample showed no broad peak ascribable to c-ESR. The fraction of the $A15$ phase is 31%. The value of ρ for this sample is 5×10^{-1} Ω cm at 300 K, which is larger by two orders than those of K_3C_{60} (5.2×10^{-3} Ω cm) and Rb_3C_{60} (4.7×10^{-3} Ω cm).[21] In K_3C_{60} and Rb_3C_{60}, ρ increases linearly with an increase in temperature above T_c,[22,23] implying that K_3C_{60} and Rb_3C_{60} are normal metals above T_c. On the other hand, ρ for the $Cs_{3.5(1)}C_{60}$ sample decreases with an increase in temperature; the ρ value is higher than 10^4 Ω cm below 50 K. The plots of $\ln \rho$ vs $1/T$ for the $Cs_{3.5(1)}C_{60}$ samples are shown in Figs. 9(b). The plots do not show a linear relationship, implying that this sample is not a normal semiconductor, while the plots of $\ln \rho$ vs $1/T^{1/2}$ show a liner relationship [Figs. 9(c)]. In the granular metal theory based on hopping conduction, the $\ln \rho$ is related to $T^{1/2}$ by the equation $\rho = \rho_0 \exp(T_0/T^{1/2})$,[24] where ρ_0 and T_0 are constants. Further, we tried to fit the plots by Sheng model based on fluctuation-induced tunneling conduction, $\rho = \rho_0 \exp[T_0/(T+T_1)]$, where T_0 and T_1 are constants.[25,26] These models can be applied to the sample consisted of metallic part and nonmetallic barri-
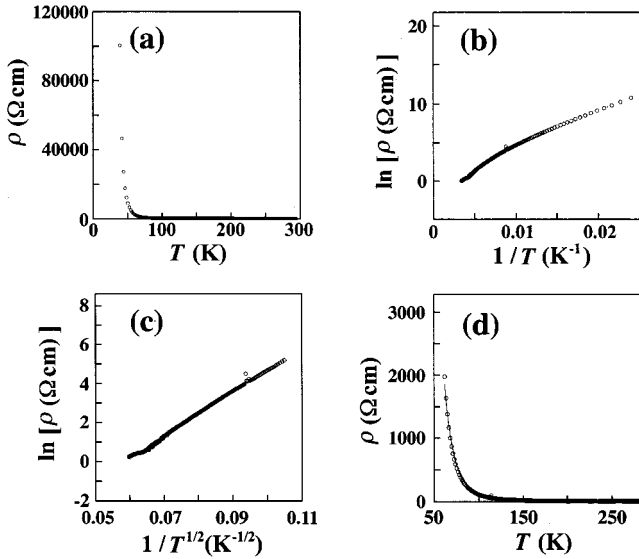
FIG. 10. Plots of (a) ρ vs T, (b) $\ln \rho$ vs $1/T$ (c) $\ln \rho$ vs $1/T^{1/2}$, and (d) ρ vs T in $Cs_{3.3(1)}C_{60}$. In (c) and (d), the fitting curves are drawn based on the equations of granular metal theory and Sheng model, respectively.

FIG. 11. ac susceptibilities of the (a) $Cs_{3.2(3)}C_{60}$ and (b) $Cs_{3.5(1)}C_{60}$ samples.

ers separating the metallic parts. The ρ plots could not completely be fitted by this equation, as seen from Fig. 9(d). The temperature dependence of ρ, for a $Cs_{3.2(3)}C_{60}$ sample exhibiting no broad ESR spectrum, was the same as that of the $Cs_{3.5(1)}C_{60}$ sample; the fraction of the $A15$ phase in the $Cs_{3.2(3)}C_{60}$ sample is 9%. The value of ρ of $Cs_{3.2(3)}C_{60}$ at 300 K was the same as that of $Cs_{3.5(1)}C_{60}$; 5×10^{-1} Ω cm. Consequently, we can point out that the normal-metallic phase does not exist in the bco $Cs_{3+\alpha}C_{60}$ ($\alpha \neq 0.0$) and the $A15$ phases.

ρ of the $Cs_{3.3(1)}C_{60}$ sample exhibiting a broad ESR peak [Fig. 7(b)] was also measured [Fig. 10(a)]. The ρ plots did not show a linear relationship, which is expected for a normal metal, as in the $Cs_{3.2(3)}C_{60}$ and $Cs_{3.5(1)}C_{60}$ samples exhibiting no broad ESR peak. Further, the plots of $\ln \rho$ vs $1/T$ did not show a liner relationship [Fig. 10(b)]. The plots can be well fitted by $\rho = \rho_0 \exp(T_0/T^{1/2})$, as shown in Fig. 10(c). Further, the plots could be fitted by Sheng model [Fig. 10(d)], which is different from the results for the $Cs_{3.2(3)}C_{60}$ and $Cs_{3.5(1)}C_{60}$ samples. This may be associated with the fact that the $Cs_{3.3(1)}C_{60}$ sample exhibits a broad ESR peak. However, the value of ρ was the same as that of the $Cs_{3.2(3)}C_{60}$ and $Cs_{3.5(1)}C_{60}$. Consequently, the direct measurements of ρ did not show a normal-metallic behavior for any samples of $Cs_{3+\alpha}C_{60}$ ($\alpha \neq 0.0$), though the possibility of normal metal was suggested for the $Cs_{3.3(3)}C_{60}$ sample from ESR.

The ac susceptibility of the $Cs_{3.2(1)}C_{60}$ and $Cs_{3.5(1)}C_{60}$ samples under high pressure are shown in Figs. 11(a) and 11(b), respectively; these samples show neither a broad ESR peak nor a linear relationship in ρ vs T plots. The applied pressures were 6.9 kbar for $Cs_{3.2(3)}C_{60}$ and 8.1 kbar for $Cs_{3.5(1)}C_{60}$. No superconducting transition was observed in the temperature region from 1.3 to 300 K for both samples. This result shows that the bco phase of $Cs_{3+\alpha}C_{60}$ ($\alpha \neq 0.0$) is not a superconducting phase under high pressure. Further,
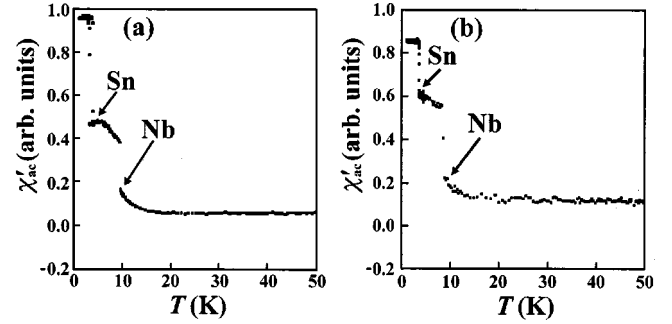
this suggests that the $A15$ phase is also not a superconducting phase under high pressure, because these samples contain 9–31% of the $A15$ phase. Further, no superconducting transition was observed up to 10.6 kbar, even in $Cs_{3.3(1)}C_{60}$ exhibiting a broad ESR peak. The superconducting transition may be suppressed in $Cs_{3.3(1)}C_{60}$ owing to the existence of a nonmetallic barrier between metallic parts, suggested from a good fit by Sheng model [Fig. 10(d)]. Consequently, we present the bco $Cs_{3+\alpha}C_{60}$ ($\alpha = 0.0$) phase as a final candidate of a metallic and pressure-induced superconducting phase.

In the present work, the bco phases of $Cs_{3+\alpha}C_{60}$ ($\alpha = 0.0$–1.0) and the $A15$ phase of Cs_3C_{60} have been studied under ambient and high pressures. No structural phase transition was observed for the bco phases of $Cs_{3+\alpha}C_{60}$ up to 50 kbar and down to 11 K. The fraction of the $A15$ phase decreased gradually, with an increase in pressure and vanished above 30 kbar. This results neglect the model of pressure-induced superconductivity based on the assumption that the structural phase transition occurs from bco to cubic phase at high pressure. The ESR suggested the possibility of normal metal for the bco phase of $Cs_{3+\alpha}C_{60}$ ($\alpha \sim 0.0$), while the ρ for the $Cs_{3+\alpha}C_{60}$ ($\alpha \neq 0.0$) samples at 1 bar was larger by two orders than those of K_3C_{60} and Rb_3C_{60},[21] even when the broad ESR peak was observed. The superconducting transition in the bco phase of $Cs_{3+\alpha}C_{60}$ ($\alpha \neq 0.0$) and the $A15$ phase was not observed down to 1.3 K even under high pressure. The fact that a superconducting transition is observed neither in the bco $Cs_{3+\alpha}C_{60}$ ($\alpha \neq 0.0$) phase nor the $A15$ phase seems to be reasonable, because these phases are not normal metals above 40 K at 1 bar, as suggested from direct ρ measurements.

ACKNOWLEDGMENTS

*Author to whom correspondence should be addressed. Email address: kubozono@ims.ac.jp

[1] O. Zhou, G. B. M. Vaughan, Q. Zhu, J. E. Fischer, P. A. Heiney, N. Coustel, J. P. McCauley, Jr., and A. B. Smith III, Science **255**, 833 (1992).

[2] C. M. Brown, T. Takenobu, K. Kordatos, K. Prassides, Y. Iwasa, and K. Tanigaki, Phys. Rev. B **59**, 4439 (1999).

[3] R. M. Fleming, A. P. Ramirez, M. J. Rosseinsky, D. W. Murphy, R. C. Haddon, S. M. Zahurak, and A. V. Makhija, Nature (London) **352**, 787 (1991).

[4] T. T. M. Palstra, O. Zhou, Y. Iwasa, P. E. Sulewski, R. M. Fleming, and B. R. Zegarski, Solid State Commun. **93**, 327 (1995).

[5] Y. Yoshida, Y. Kubozono, S. Kashino, and Y. Murakami, Chem. Phys. Lett. **291**, 31 (1998).

[6] P. Dahlke, P. F. Henry, and M. J. Rosseinsky, J. Mater. Chem. **8**, 1571 (1998).

[7] F. Izumi, in *The Rietveld Method*, edited by R. A. Young (Oxford University Press, New York, 1993), p. 236.

[8] Y.-I. Kim and F. Izumi, J. Ceram. Soc. Jpn. **102**, 401 (1994).

[9] H. K. Mao, P. M. Bell, J. W. Shaner, and D. J. Steinberg, J. Appl. Phys. **49**, 3276 (1978).

[10] A. R. Kortan, N. Kopylov, R. M. Fleming, O. Zhou, F. A. Thiel, R. C. Haddon, and K. M. Rabe, Phys. Rev. B **47**, 13 070 (1993).

[11] K. Umemoto (private communication).

[12] P. Zhou, K.-A. Wang, P. C. Eklund, G. Dresselhaus, and M. S. Dresselhaus, Phys. Rev. B **48**, 8412 (1993).

[13] S. J. Duclos, R. C. Haddon, S. Glarum, A. F. Hebard, and K. B. Lyons, Science **254**, 1625 (1991).

[14] M. G. Mitch and J. S. Lannin, Phys. Rev. B **51**, 6784 (1995).

[15] Y. Kubozono, S. Fujiki, Y. Takabayashi, Y. Yoshida, S. Kashino, K. Ishii, A. Fujiwara, and H. Suematsu, in *Electronic Properties of Novel Materials-Science and Technology of Molecular Nanostructures*, edited by H. Kuzmany, J. Fink, M. Mehring, and S. Roth (AIP, New York, 1999), p. 69.

[16] S. Fujiki, Y. Kubozono, S. Emura, Y. Takabayashi, S. Kashino, A. Fujiwara, K. Ishii, H. Suematsu, Y. Murakami, Y. Iwasa, T. Mitani, and H. Ogata, Phys. Rev. B **62**, 5366 (2000).

[17] Y. Kubozono, S. Fujiki, K. Hiraoka, T. Urakawa, Y. Takabayashi, S. Kashino, Y. Iwasa, H. Kitagawa, and Y. Mitani, Chem. Phys. Lett. **298**, 335 (1998).

[18] P. Petit, J. Robert, T. Yildirim, and J. E. Fischer, Phys. Rev. B **54**, R3764 (1996).

[19] R. J. Elliott, Phys. Rev. **96**, 266 (1954).

[20] Y. Yafet, in *Solid State Physics*, edited by H. Ehrenreich, F. Seitz, and D. Turnbull (Academic, New York, 1963), Vol. 14, p. 1.

[21] F. Stepniak, P. J. Benning, D. M. Poirier, and J. H. Weaver, Phys. Rev. B **48**, 1899 (1993).

[22] X.-D. Xiang, J. G. Hou, G. Briceño, W. A. Vareka, R. Mostovoy, A. Zettl, V. H. Crespi, and M. L. Cohen, Science **256**, 1190 (1992).

[23] X.-D. Xiang, J. G. Hou, V. H. Crespi, A. Zettl, and M. L. Cohen, Nature (London) **361**, 54 (1993).

[24] P. Sheng, B. Abeles, and Y. Arie, Phys. Rev. Lett. **31**, 44 (1973).

[25] P. Sheng, E. K. Sichel, and J. L. Gitteleman, Phys. Rev. Lett. **40**, 1197 (1978).

[26] P. Sheng, Phys. Rev. B **21**, 2180 (1980).